Long Distance/Duration Trajectory Optimization for Small UAVs

Jack W. Langelaan*

The Pennsylvania State University, University Park, PA 16802, USA

This paper presents a system for autonomous soaring flight by small and micro uninhabited aerial vehicles. It combines a prediction of wind field with a trajectory planner, a decision-making block, a low-level flight controller and sensors such as Global Positioning System and air data sensors to enable exploitation of atmospheric energy using thermals, wave, and orographic lift or dynamic soaring.

The major focus of this research is on exploiting orographic (i.e. slope or ridge) lift to enable long duration, long distance flights by a small autonomous uninhabited aerial vehicle (UAV). This paper presents a methodology to generate optimal trajectories that utilize the vertical component of wind to enable flights that would otherwise be impossible given the performance constraints of the UAV. A point mass model is used to model the aircraft and a polynomial function which includes both horizontal and vertical variations in wind speed is used to model the wind field. Both vehicle kinematic and minimum altitude constraints are included. Results for a test case (crossing the Altoona Gap in Pennsylvania's Bald Eagle Ridge) are presented for both minimum time and maximum final energy trajectories.

I. Introduction

A MAJOR LIMITATION in developing practical small uninhabited aerial vehicles (UAV) is the energy required for long-range, long endurance operations. Large aircraft such as the Global Hawk can remain on-station for 24 hours and can fly non-stop from the continental United States to Australia. However, small and micro UAVs face severe limits on the fuel that can be carried, greatly reducing both endurance and range. In addition, the best L/D attainable for small and micro UAVs is typically much smaller than for larger aircraft because of the smaller Reynolds numbers. This further reduces performance.

Significant range and endurance improvements can be realized by obtaining energy (in the form of altitude or speed) from the surrounding atmosphere. Energy can be obtained from vertical air motion, from velocity gradients and from gusts. Vertical air motion has three main causes: uneven heating of the ground, which produces buoyant instabilities known as thermals; long period oscillations of the atmosphere, generally called wave; and orographic lift, where wind is deflected by the slopes of hills and mountains. Vertical air motion is a quasi-static phenomenon, and flight which exploits vertical air motion is known as soaring. Large birds such as eagles, hawks and condors as well as human sailplane and hang glider pilots routinely use soaring flight to remain aloft for many hours and traverse hundreds of kilometers without flapping wings or the use of engines.

A second means of extracting energy from the air uses velocity gradients (which can occur near the ground due to the boundary layer) or shear layers (which often occur on the leeward side of mountains and ridges). This strategy, called dynamic soaring, was first described by Lord Rayleigh in an analysis of albatross flight.[1,2] Dynamic soaring is again becoming the subject of research both for recreational flight (mainly by RC flying enthusiasts) and for UAV flight. However, this class of dynamic soaring generally requires highly agile flight in close proximity to the ground: this is a very risky endeavor.

The third means of extracting energy from the air exploits gusts. It has been observed that the flight performance of large birds is improved by gusts, while it is typically reduced on human-piloted aircraft.[3] This suggests that birds are able to extract energy from gusts, and indeed Kiceniuk reports that it is even

---

*Assistant Professor, Department of Aerospace Engineering, Senior Member AIAA.

possible to extract energy from a downward gust[4]! Extracting energy from gusts is complicated by their typically short duration, hence very fast response (typically exceeding human reaction time) is required. Control laws have been developed to enable energy extraction from gusts by small UAVs.[5]

These three methods of extracting energy from the environment can be used to enable autonomous long duration, long distance flight (denoted $(LD)^2$ flight) by unmanned aerial vehicles. For the remainder of this paper these three modes of energy extraction will be referred to as static soaring, dynamic soaring and gust soaring, respectively.

The time scales of each of these modes of flight are very different. Static soaring occurs over time ranging from minutes to hours, dynamic soaring typically consists of a periodic trajectory with a duration of a few tens of seconds and gusts are very short duration (less than a few seconds). In a system which exploits all three modes of energy extraction this time scale separation can be used to treat each mode almost independently. Long-duration planning can be performed to exploit spatial variation in wind speed (both vertical and horizontal), shorter duration optimal trajectories can be designed for dynamic soaring and a closed-loop controller can be designed to exploit gusts.

The major focus of this paper is on the problem of static soaring by a small UAV specifically on enabling both long endurance and long range flights using orographic (i.e. slope) lift. It describes a planning algorithm which uses a point mass model of the vehicle and knowledge of the wind field (this may be obtained from predictions generated using meteorological forecasting tools such as MM5[6]) to generate trajectories which optimize a particular cost or reward function (such as maximizing energy gain or minimizing the time required to reach a goal).

The remainder of this paper is organized as follows. Section II describes previous and related research. Section III introduces and briefly describes a system which enables exploitation of atmospheric phenomena by small autonomous aircraft. Section IV discusses the dynamics of soaring using orographic lift and briefly investigates the variation of energy with respect to altitude for some constant airspeed, constant altitude trajectories for flight along an infinite cylindrical ridge. Section V describes the planning algorithm and discusses some cost functions. Section VI presents results of a sample problem: flight along a ridge with a gap. The gap crossing problem illustrates the effect of cost function on the optimal trajectory and the effect of aircraft wing loading on the optimal trajectory. Finally Section VII presents concluding remarks.

II.   Previous and Related Work

DYNAMIC SOARING HAS been studied for some time.[7] Both required wind strength[8,9] and optimal flight patterns have been studied.[10] Heuristics for flight control for autonomous dynamic soaring are described by Wharington.[11] An extensive study of dynamic soaring along with flight test data of human-piloted dynamic soaring in the lee of a ridge is reported.[3] Woolsey[12] discusses both dynamic soaring and buoyancy driven flight for exploration of Venus and Titan. Kiceniuk[4,13,14] provides a fairly intuitive discussion of dynamic soaring: he discusses energy gain from gusts and the information required to exploit gusts, which indicates the necessary sensing for such flight modes.

In addition, dynamic soaring by birds has been studied extensively. The minimum wind shear strength required for albatross flight is discussed by Sachs.[9] Pennycuick[15] proposes an alternate flight mode where most of the energy gain is obtained from the shear layer which results from the winds flow separation over the crest of each wave. Successful exploitation of this strategy requires sensing very small changes in dynamic pressure, and he suggests that only tube-nosed birds such as albatrosses have the necessary sensory capability.

Autonomous static soaring is now becoming the focus of more research. Simulation results of thermal flight are reported by Allen (2005)[16] and flight test results are presented in Allen (2007).[17] Energy gain from orographic lift is not addressed, nor is energy gain from gusts.

A rich and varied literature exists in the field of optimal static soaring trajectories with the application of human-piloted soaring flight. Various aspects of optimal static soaring have been addressed, including the optimal speed to fly between thermals of known strength (the MacCready problem,[18,19] the final glide problem,[20] and "dolphin" flight along regions of alternating lift and sink.[21–23] de Jong[24] describes a geometric approach to trajectory optimization and also discusses the optimal deviation from course to minimize time to a goal in a given lift field. Much of this research is directly applicable to the problem of trajectory generation for autonomous soaring flight, but it assumes limited types of known lift distributions (e.g. sinusoidally varying lift[25] or "square wave" lift[26]) and it assumes that the vertical wind speed does not vary with altitude. These assumptions are adequate for planning trajectories which exploit thermal lift, but they

do not generally apply to the problem considered in this paper (i.e. exploiting orographic lift).

Trajectory optimization for UAVs is an active area of research. Typical applications include minimal altitude trajectories for nap of the earth flight[27] or flight in urban environments.[28] The major difference in the present research is the use of planning algorithms to enable performance which would not be otherwise realizable (i.e. $(LD)^2$ flight) given the performance and payload limitations of a small UAV.

III.   Exploiting Atmospheric Energy

A HIGH-LEVEL BLOCK diagram of a system capable of autonomous energy extraction is shown in Figure 1. While this paper is focused on the problem of extracting energy from orographic lift, the block diagram is applicable to general static soaring flight (i.e. thermal, orographic and wave soaring), dynamic soaring and gust soaring.
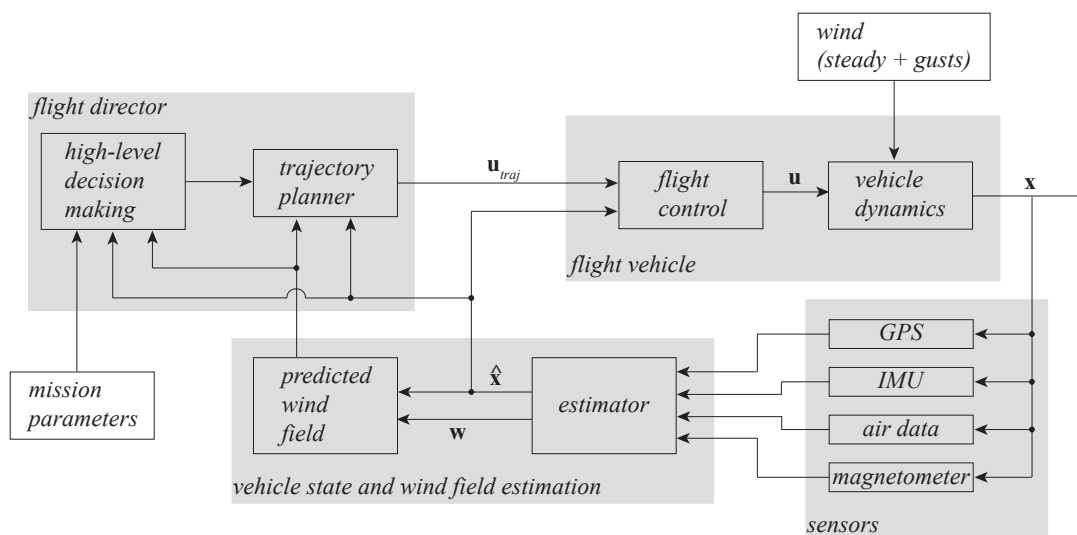

Figure 1.   High-level block diagram of system for autonomous soaring flight.

Mission parameters (such as regions that must be visited or avoided, time constraints) are determined by the human operator and form the top-level input to the system. The flight director includes high-level decision making and a trajectory planner. The decision making block is responsible for monitoring flight progress based on mission parameters and vehicle state, and decides on the flight mode based on mission parameters, the predicted wind field and vehicle state.

Flight modes may consist of soaring strategies, i.e. thermal soaring, orographic/wave soaring, dynamic soaring or powered flight. The flight mode would be determined in part by the predicted wind field and can change based on updates in mission parameters, expected availability of certain types of lift or mission progress.

The trajectory planner selects a trajectory class based on flight mode and plans a trajectory based on predicted wind field, current vehicle state and the goal. For thermal flight mode the trajectory plan will likely be reactive (i.e. fly on a heading at an airspeed until a thermal is encountered, then exploit the thermal) because it is beyond current capabilities to accurately predict thermal formation. The availability of specialized sensors which can 'see' thermals (e.g. forward-looking infrared sensors) would greatly improve performance in this flight mode. Techniques based on MacCready theory would be used to determine flight speed and determine whether to exploit or ignore a particular thermal, and Allen's thermal soaring controller[17] could be used when the decision to exploit a thermal has been made. Trajectory planning for orographic, wave and dynamic soaring can take advantage of a priori knowledge of the wind field.

The flight controller stabilizes vehicle dynamics and follows commands from the trajectory generator. It may also include the ability to extract energy from short duration atmospheric phenomena such as gusts. Gust soaring has the potential to greatly improve flight performance of small UAVs[29] and is becoming an

active area of research.[5, 30]

The predicted wind field can be initialized using data from meteorological simulations such as MM5[6] or WRF.[31] The wind field can be updated in flight using in situ measurements taken by the aircraft. In the meteorological community this is known as *assimilation,* and this is an active area of research.[32]

The remainder of this paper is focused on the problem of trajectory planning for a particular mode of soaring flight, namely orographic (i.e. ridge) soaring. It discusses the kinematics and dynamics of ridge soaring, derives a simplified kinematic model suitable for long-range planning and presents a solution for flight along a ridge with a gap.

IV.   Dynamics of Ridge Soaring

THIS SECTION PRESENTS an overview of the dynamics of ridge soaring using a point mass model. Ultimately airspeed is used as the control input, leading to a kinematic model. This is a common approach in analysis of optimal soaring trajectories, and the critical assumption is that the aircraft is in equilibrium at all times during the trajectory. This assumption is adequate as long as the periods of transition between segments of constant airspeed are short compared with the length of the segments.

Figure 2 shows a schematic of a point mass model of an aircraft in steady flight. An inertial coordinate frame is defined by unit vectors $\hat{\mathbf{x}}^i$ and $\hat{\mathbf{z}}^i$ and the flight path angle is denoted γ. Forces acting on the aircraft are thrust T, drag D, lift L, and gravity mg.

Resolving forces parallel and perpendicular to the flight path,

$$mg\cos\gamma = L + T\sin\alpha \tag{1}$$
$$mg\sin\gamma = D - T\cos\alpha \tag{2}$$

where m is mass of the vehicle and α is the angle of attack.

It is assumed that the flight path angle γ is small, hence $\sin\gamma \approx \gamma$ and $\cos\gamma \approx 1$. A further simplifying assumption (admittedly less accurate) is that thrust is always aligned with the flight path angle (i.e. α is zero). From Equation 1

$$mg = L = \frac{1}{2}\rho v_a^2 S C_L \tag{3}$$

therefore

$$C_L = \frac{2mg}{\rho v_a^2 S} \tag{4}$$

Figure 2.   Point mass model.

Here C_L is lift coefficient, ρ is density of the air, v_a is airspeed and S is wing area. A second order approximation is used for the aircraft's drag polar:

$$C_D = a_0 + a_1 C_L + a_2 C_L^2 \tag{5}$$

Thus the drag force is

$$D = \frac{1}{2}\rho v_a^2 S \left(a_0 + a_1 C_L + a_2 C_L^2\right) \tag{6}$$

Substituting into Equation 2, the flight path angle for a particular speed and thrust can thus be computed as

$$mg\gamma = \frac{1}{2}\rho v_a^2 S \left(a_0 + a_1 C_L + a_2 C_L^2\right) - T \tag{7}$$

The kinematics of the aircraft can now be defined in terms of the airspeed, flight path angle and wind speed.

$$\dot{x}_i = v_a\cos\gamma + w_x \tag{8}$$
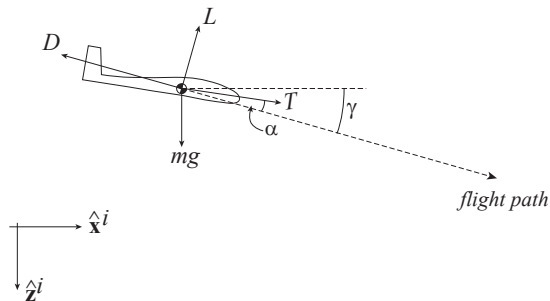$$\dot{z}_i = v_a\sin\gamma + w_z \tag{9}$$

where $\dot{x}_i$ and $\dot{z}_i$ are components of velocity in the inertial x and z directions, respectively.

The wind speed is modelled using a polynomial function of position in the inertial frame:

$$\mathbf{w} = f(x_i, z_i) \tag{10}$$

The aircraft trajectory defined by Equations 7 through 10 can be completely determined by airspeed v_a and thrust T. For an aircraft equipped with flaps it is assumed that the effect of flaps on drag is incorporated in a low-level controller. A flap setting can then chosen to minimize drag (in cruise flight) or to permit higher angle of attack (in low speed flight). Note that while the kinematic formulation described can be used to model static soaring flight (thermal, ridge and wave), it is not adequate to model dynamic soaring.

A. Vehicle Energy

An expression for total energy in terms of airspeed and windspeed can now be obtained. Ignoring stored energy (i.e. fuel or electrical energy stored in batteries), total energy is

$$E = mgh + \frac{m(\dot{x}_i^2 + \dot{z}_i^2)}{2} \tag{11}$$

where h is altitude. Substituting vehicle kinematics (Equation 8 and Equation 9) gives

$$E = mgh + \frac{1}{2}m\left((v_a \cos\gamma + w_x)^2 + (v_a \sin\gamma + w_z)^2\right) \tag{12}$$

hence

$$E = mgh + \frac{1}{2}m\left(v_a^2 + 2w_x v_a \cos\gamma + 2w_z v_a \sin\gamma + w_x^2 + w_z^2\right) \tag{13}$$

B. Constant Altitude Trajectories

For illustrative purposes an idealized case of soaring along an infinite cylindrical ridge is briefly considered. A schematic is shown in Figure 3, where an infinitely long semi-cylindrical ridge with radius R is oriented along the $\hat{\mathbf{x}}^i$ axis.

A glider flies at constant airspeed along the ridge. By flying in a region where the vertical component of wind is equal to the sink rate constant altitude can be maintained. The total energy for a particular altitude will be computed.

Potential flow is used to generate a wind field:

$$\mathbf{w} = -w_\infty \hat{\mathbf{y}}^i - w_\infty \frac{R^2}{r^2}\left(\cos\eta\,\hat{\mathbf{r}} - \sin\eta\,\hat{\boldsymbol{\eta}}\right) \tag{14}$$

where w_∞ is the wind speed far from the ridge. The vertical component of wind speed is

$$w_z = -\hat{\mathbf{z}}^i \cdot w_\infty \frac{R^2}{r^2}\left(\cos\eta\,\hat{\mathbf{r}} - \sin\eta\,\hat{\boldsymbol{\eta}}\right) \tag{15}$$

hence

$$w_z = -2w_\infty \frac{R^2}{r^2}\cos\eta\sin\eta \tag{16}$$

Figure 3. Soaring along an infinite semi-cylindrical ridge.

The vertical component of wind speed is greatest along the radial at $\eta = 45°$, where $w_z = -w_\infty R^2/r^2$. Constant altitude, constant velocity trajectories will be computed for a glider flying parallel to the ridge on this radial, and the total energy will be computed.

For a constant altitude trajectory $\dot{z} = 0$, hence $v_a \sin\gamma = -w_z$. From Equation 4 and Equation 6:

$$-w_z = \frac{\rho S a_0}{2mg}v_a^3 + a_1 v_a + \frac{2mg a_2}{\rho S v_a} \tag{17}$$

where a_i are the coefficients of the second-order lift-drag polar (Equation 5).
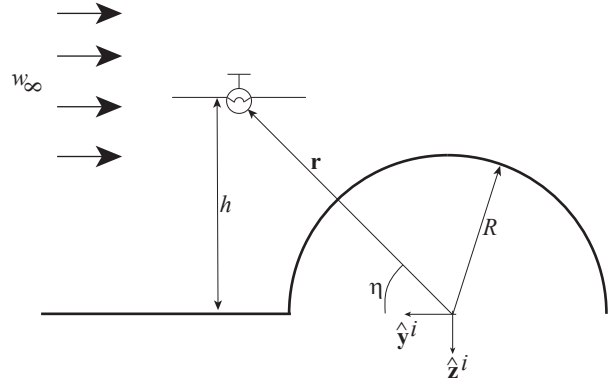
Table 1. Glider parameters.

parameter	description	value
S	wing area	1 m^2
a	C_D vs. C_L	[0.0264 -0.0090 0.0150]

Since the glider is assume to remain on the radial $\eta = 45°$ the vertical component of windspeed for a particular altitude h can be calculated. The airspeed for constant altitude flight can be obtained by solving

$$w_\infty \frac{R^2}{2h^2} = \frac{\rho S a_0}{2mg} v_a^3 + a_1 v_a + \frac{2mga_2}{\rho S v_a} \tag{18}$$

The total energy at a particular altitude can then be obtained from

$$E = mgh + \frac{1}{2}m\left(v_a^2 - w_z^2\right) \tag{19}$$

where $w_x = 0$ and $v_a \sin\gamma = -w_z$ have been substituted into Equation 13.

Constant altitude trajectories were computed for a small autonomous glider with parameters given in Table 1 for three different values of mass: 10kg, 20kg and 30kg. For comparison a modern high-performance glider (Glaser-Dirks DG-808S[33] with wing loading 30kg/m^2) is also shown. Figure 4 shows the resulting lift/drag and velocity polar. Note the effect of wing loading on the glider's sink rate: best L/D (and the speed of best L/D) increase with wing loading, as does minimum sink rate and the speed of minimum sink. This in turn will affect the constant altitude speeds that can be flown at a given altitude.

Results showing variation in total energy with altitude and variation of airspeed with altitude are plotted in Figure 5. For all aircraft maximum energy flight occurs at high altitude. The sailplane shows a clear minimum in total energy at an intermediate altitude. At very low altitude (where the vertical component of wind speed is greatest) very high air speed can be flown while maintaining constant altitude, so kinetic energy becomes dominant in the total energy. Note that the high performance sailplane can fly at significantly higher speeds than the small UAV for a similar sink rate, increasing this effect significantly.
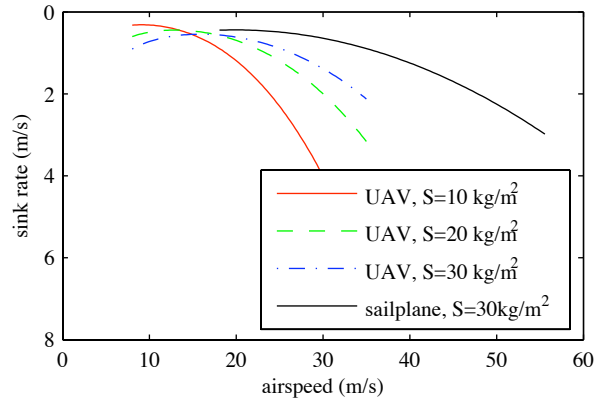

Figure 4. Speed polar (sink rate vs. airspeed) for small autonomous glider at varying wing loadings. For comparison a polar for a high-performance sailplane is also shown.

V. Trajectory Planning

THE REMAINDER OF this paper is concerned with planning trajectories which exploit atmospheric lift. The general trajectory optimization problem can be expressed as

$$\text{minimize} \qquad C(\mathbf{x}, \mathbf{u}) \tag{20}$$

$$\text{subject to} \qquad \dot{\mathbf{x}} = f(\mathbf{x}, \mathbf{u}, \mathbf{w}) \tag{21}$$

$$\mathbf{x}_{min} \le \mathbf{x} \le \mathbf{x}_{max} \tag{22}$$

$$\mathbf{u}_{min} \le \mathbf{u} \le \mathbf{u}_{max} \tag{23}$$

where C is a cost function (discussed below), Equation 21 defines constraints on vehicle dynamics, Equation 22 defines constraints on the state (for example minimum altitude or minimum/maximum airspeed), and finally Equation 23 defines constraints on control inputs (for example control surface deflections).

In this work a kinematic model is used for the vehicle and control inputs are airspeed and thrust. State constraints (such as minimum altitude) can also be incorporated as a barrier function in the cost.
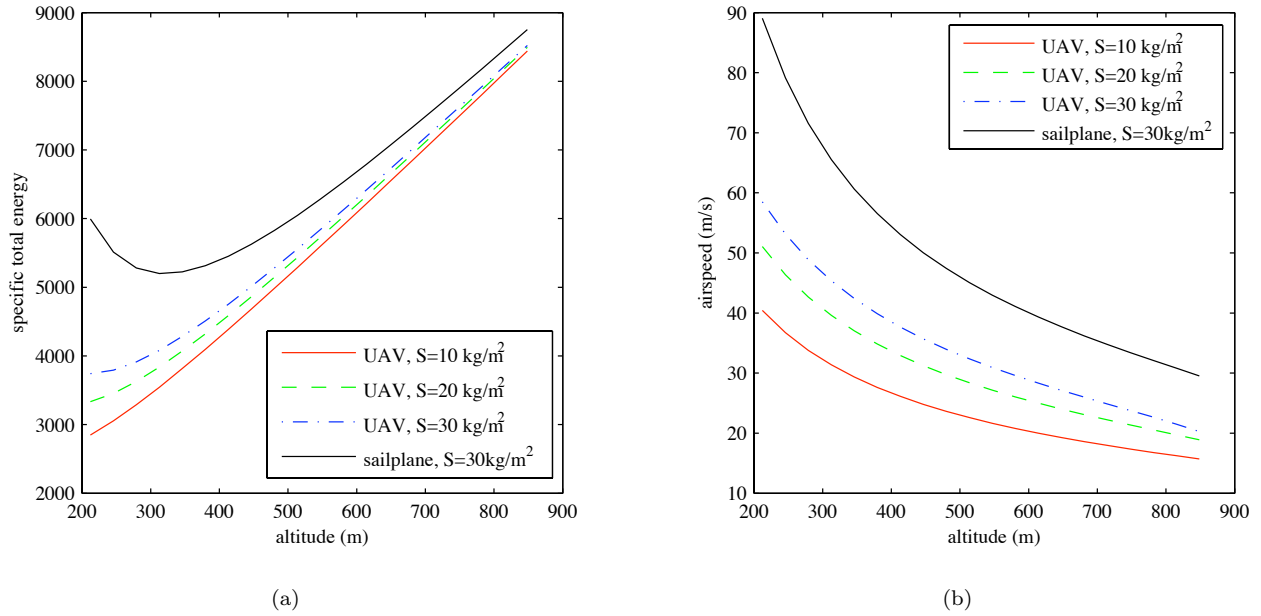
Figure 5. Constant altitude soaring along an infinite cylindrical ridge. The left figure shows normalized total energy (energy/mass), the right figure shows airspeed. In both cases results are plotted for varying wingloading.

A. Discretization

The continuous time optimization problem is discretized in x to generate a vector optimization problem. This is shown in Figure 6.

Note that each segment Δx_k is not necessarily of equal length: this allows tighter discretization in areas where the wind speed is changing rapidly. The total number of segments used to discretize a trajectory can be chosen depending in part on computational considerations, but overly coarse discretization will reduce the quality of the solution. On the other hand, if the discretization is too fine then the earlier assumption that kinematics are an adequate model of the glider becomes suspect.

Wind speed is modelled using a polynomial function of altitude. Within a particular segment this polynomial is assumed to be constant.

$$w_x^{(k)} = c_{x,0}^{(k)} + c_{x,1}^{(k)}\tilde{h} + c_{x,2}^{(k)}\tilde{h}^2 + \cdots \quad (24)$$

$$w_z^{(k)} = c_{z,0}^{(k)} + c_{z,1}^{(k)}\tilde{h} + c_{z,2}^{(k)}\tilde{h}^2 + \cdots \quad (25)$$

Figure 6. Discretized trajectory optimization problem. The heavy black line denotes terrain, wind vectors are shown as grey arrows.

where $\tilde{h} = h/H_{wind}$ is a normalized height above terrain and the superscript (k) denotes a particular segment. Within the limits of discretization and the polynomial function arbitrary wind distributions can thus be modelled. The variable H_{wind} is a scale height which defines the maximum height of validity for the polynomial wind field.

The time required to fly a segment is computed using vehicle kinematics (Equation 8):

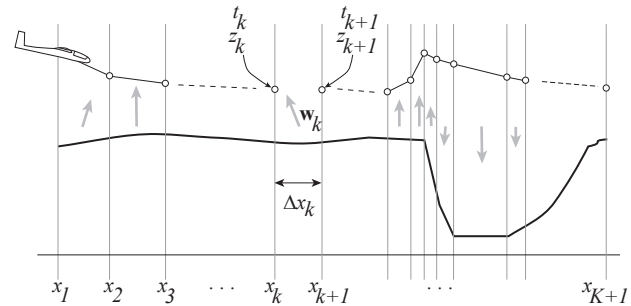$$\Delta t_k = \frac{\Delta x_k}{\dot{x}_k} \quad (26)$$

American Institute of Aeronautics and Astronautics Paper 2007-6737

and time and altitude are computed as

$$t_{k+1} = t_k + \Delta t_k \tag{27}$$

$$z_{k+1} = z_k + \dot{z}_k \Delta t_k + \Delta z_k \tag{28}$$

where $\dot{z}_k$ is given in Equation 9.

Recall that a kinematic model is used for the vehicle. The kinematic model does not include the dynamics relating changes in airspeed and altitude. This exchange is reflected in the quantity Δz_k in Equation 28. Assuming that the duration of the speed change is short compared with the time required to fly a segment and that total energy is constant during a speed change, the change in altitude due to a change in speed is

$$\Delta z_k = \frac{v_{a,k}^2 - v_{a,k+1}^2}{2g} \tag{29}$$

To summarize, the discretized trajectory optimization problem is

$$\text{minimize} \quad C(\mathbf{v}_a, \mathbf{T}) \tag{30}$$

$$\text{subject to} \quad v_{min} \leq v_{a,k} \leq v_{max} \tag{31}$$

$$\gamma_k = \frac{\rho S v_{a,k}^2}{2gm}\left(a_0 + a_1 C_L + a_2 C_L^2\right) - \frac{T_k}{mg} \tag{32}$$

$$\dot{x}_k = v_{a,k} \cos\gamma_k + w_x^k \tag{33}$$

$$\dot{z}_k = v_{a,k} \sin\gamma_k + w_z^k \tag{34}$$

$$\Delta t_k = \frac{\Delta x_k}{\dot{x}_k} \tag{35}$$

$$t_{k+1} = t_k + \Delta t_k \tag{36}$$

$$z_{k+1} = z_k + \dot{z}_k \Delta t_k + \frac{v_{a,k}^2 - v_{a,k+1}^2}{2g} \tag{37}$$

The optimization occurs over the vectors $\mathbf{v}_a$ (airspeed in each segment) and $\mathbf{T}$ (thrust in each segment). The cost function C also includes constraints such as height above terrain as an exponential barrier function.

Note that for an electric vehicle a generator can be used to recharge batteries. This energy harvesting can be incorporated by allowing negative values of thrust and including a term reflecting stored electrical energy in the cost function C. The remainder of this paper is focused on pure gliding flight

B. Choice of Cost/Reward Functions

The choice of a cost (or equivalently, reward) function depends on the desired outcome of the flight. For gliders the goal is typically minimizing the time required to reach a goal or maximizing range. Two cost functions will therefore be considered: minimum time trajectories and trajectories which maximize total energy.

For minimum time trajectories the cost function is

$$C = \sum_{k=1}^{k=K} \left(t_k + e^{-2(h_k - h_{min,k})}\right) \tag{38}$$

The exponential term is a barrier function to maintain separation from the ground. Here h_k is altitude (i.e. $h_k = -z_k$) and $h_{min,k}$ is the minimum desired altitude for that segment, which includes height of terrain and a safety zone.

For maximum energy flight the total energy at the end of the trajectory is considered:

$$C = gh_K + \frac{1}{2}(\dot{x}_K^2 + \dot{z}_K^2) + \sum_{k=1}^{k=K} e^{-2(h_k - h_{min,k})} \tag{39}$$

where the subscript K denotes the end of the last segment.

Other cost functions may emphasis minimizing deviation from some desired altitude or reaching the goal at a desired time. Ultimately the choice of cost function is mission dependent.

VI.   Simulation

ONE OF THE critical phases of ridge soaring is crossing a gap in the ridge (where the vertical component of wind speed is zero, or worse, downwards). In this case the glider must either have obtained enough energy (i.e. speed and altitude) to cross the gap before arrival or it must find sufficiently strong thermals in the gap to enable continued flight.

An example known to glider pilots flying along the Bald Eagle Ridge in Pennsylvania is the Altoona Gap,[34] which spans approximately 10km. The height of the ridge at each end of the gap is approximately 400m above the valley floor. Figure 7 shows a satellite view. The flight originates at a point approximately 60km NorthEast of Altoona (from Ridge Soaring gliderport) and proceeds until the gap is crossed. The average height of the Bald Eagle between Ridge Soaring and the gap is somewhat lower, approximately 200m above the valley floor.

For these simulations the terrain is modelled as a 200m high ridge 60km long followed by a 10km gap. At the far side of the gap the ridge is again 200m high, which determines the minimum altitude at the end of the trajectory. The flight is discretized into equal segments 1km in length and the wind field in each segment on the ridge is

$$
\begin{aligned}
w_x &= 0 \\
w_z &= -2 + 6.55\tilde{h} - 8.14\tilde{h}^2 \\
&\quad + 0.325\tilde{h}^3 + 8.13\tilde{h}^4 - 4.88\tilde{h}^5
\end{aligned}
$$

Recall that z is positive down. In the gap wind speed is zero.

In this case pure gliding flight is considered (i.e. thrust is zero). Optimal trajectories were computed for two aircraft: a small autonomous glider (properties given in Table 1, wing loading was 10 kg/m^2)

Figure 7. Altoona Gap. The flight follows the Bald Eagle Ridge from Julian, PA to Altoona, PA. In the simplified case described in the text, ridge height is 200m and it is approximately 60km to the gap. The flight ends when the gap is crossed and the ridge is reacquired.

and a modern high performance sailplane. For these simulations MatLab's `fmincon` function was used to compute solutions on a dual processor Intel Xeon 2.79GHz desktop computer.

Optimal trajectories are generated for two cost functions: minimum time to reach the far side of the gap and maximum total energy at the far side of the gap. Results are tabulated in Table 2 and shown in Figure 8 and Figure 9.

Feasible constant speed trajectories do exist for both aircraft in the scenario considered here (this would not be true for all scenarios). Flights at best L/D (the speed for which altitude loss over a given distance is minimized) resulted in significant energy gain for both aircraft.

For both aircraft the minimum time trajectory showed significant improvement over the constant speed case. While a constant speed somewhat faster than best L/D could be flown, constant speed trajectories will quickly become infeasible (i.e. the gap will not be reached with sufficient altitude to permit safe crossing). Clearly variable speed trajectories must be flown to optimize performance. Optimal trajectories and the speed profile are shown in Figure 8. For aircraft the initial trajectory consists of a dive to fly as fast as possible just above the ridge (in the region of maximum vertical wind speed), followed by a pull-up to trade airspeed for altitude prior to crossing the gap. The small UAV's best L/D is significantly worse than the high performance sailplane (32:1 vs. 50:1), hence it requires significantly more altitude to cross the gap safely. This leads to a more aggressive pull-up maneuver prior to reaching the gap. Maximum speed is also significantly lower: this is due to the UAV's generally much higher sink rate for a given airspeed. However, the UAV did slightly increase its total energy during the flight.

Table 2. Optimal trajectory results. Values given for best L/D and sink rate are approximate.

vehicle	best L/D	minimum sink	parameter	constant speed (at best L/D)	minimum time	maximum energy
sailplane	50:1 (at 25 m/s)	0.47 m/s (at 21 m/s)	E_K/E_0	1.72	0.99	1.822
			Δz	183m	5.7m	207m
			Δt	2800s	1727s	3421s
			solution time	n/a	30 s	11 s
small UAV	32:1 (at 12 m/s)	0.2m/s (at 9 m/s)	E_K/E_0	1.69	1.06	1.91
			Δz	158m	12m	207m
			Δt	5836s	3604s	7625s
			solution time	n/a	27 s	23 s

The maximum energy trajectories showed approximately 5% improvement in energy gained over the constant speed trajectories. This is almost entirely realized in the form of higher altitude at the end of the flight, since the gap was crossed at best L/D for all the maximum energy flights. In this case the optimal flight strategy consisted of a pull-up to trade some excess initial speed for altitude followed by constant speed flight at approximately the minimum sink speed. Speed increased to best L/D to cross the gap. Since the UAV has significantly slower minimum sink speed it is not surprising it gained more altitude on the ridge, but this advantage was lost while crossing the gap: both aircraft crossed the gap at their respective best L/D and reached the far side at the same altitude. The larger gain in energy shown by the small UAV is due to the lower speed, which increases the relative importance of altitude in the total energy.

Referring back to Figure 5, we see that maximum energy for both the UAV and sailplane occur at maximum altitude when the wind profile decreases with the square of altitude (the polynomial wind field used here approximates a $1/h^2$ wind field). It is therefore not surprising that the maximum energy trajectories computed here consist of flight at low speed to gain maximum altitude followed by flight at best L/D to cross the gap. Note that it is likely that there are cases where the maximum energy trajectory closely matches a minimum time trajectory: this will depend on both the wind field and aircraft properties.
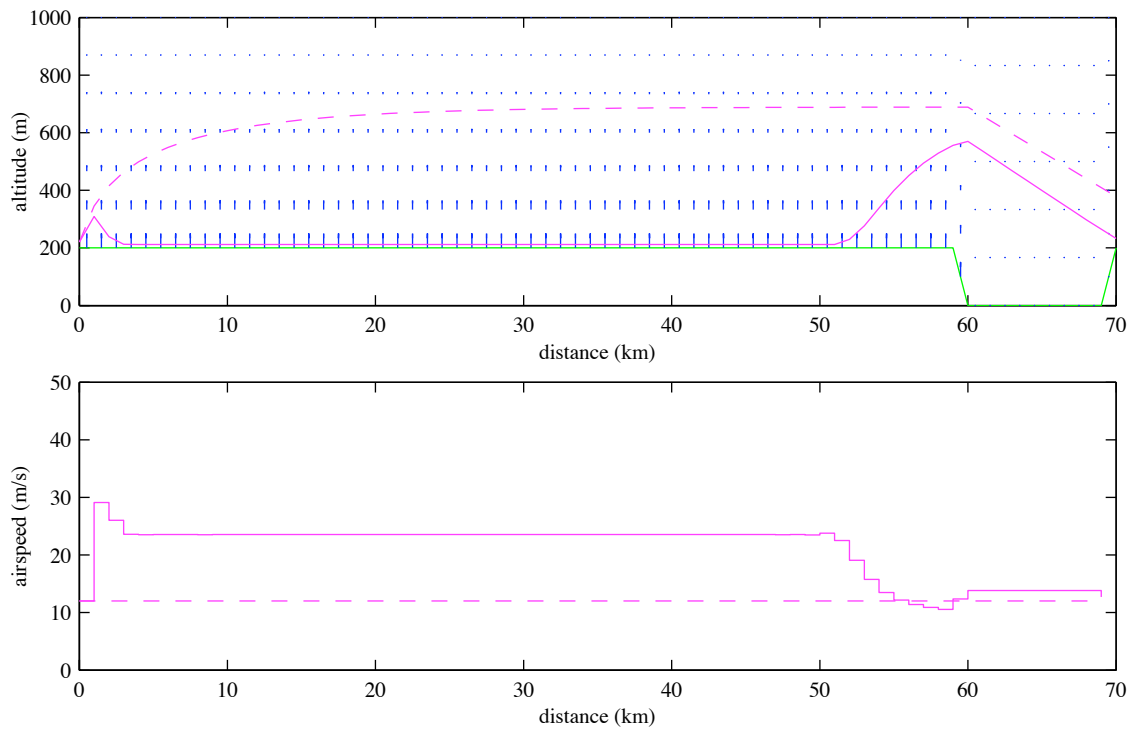
Recall the assumption of Section V that speed is generally constant during a trajectory segment (i.e. changes in speed between segments occur over a short time interval). The largest change in speed observed for both aircraft was approximately $\Delta v_a = 18$m/s (this occurs at the beginning of the minimum time trajectories as the aircraft dive to lose altitude and gain speed). The UAV flew the next segment at approximately 29 m/s, resulting in a time-to-fly of approximately 34 seconds; the sailplane flew at approximately 42 m/s for the next segment, resulting in a time-to-fly of approximately 24 seconds. For the UAV considered here, the specific drag force (D/m) in steady flight at 12m/s (the initial velocity) is 0.3 m/s^2 and at 29 m/s (speed for the next segment) is 1.27 m/s^2. Both are significantly less than the acceleration due to gravity, hence the time required to change speeds will be on the order of seconds, even for the large speed change demanded at the beginning of the flight. The assumption of constant speed over a segment is therefore adequate even for the short segments considered in this example.
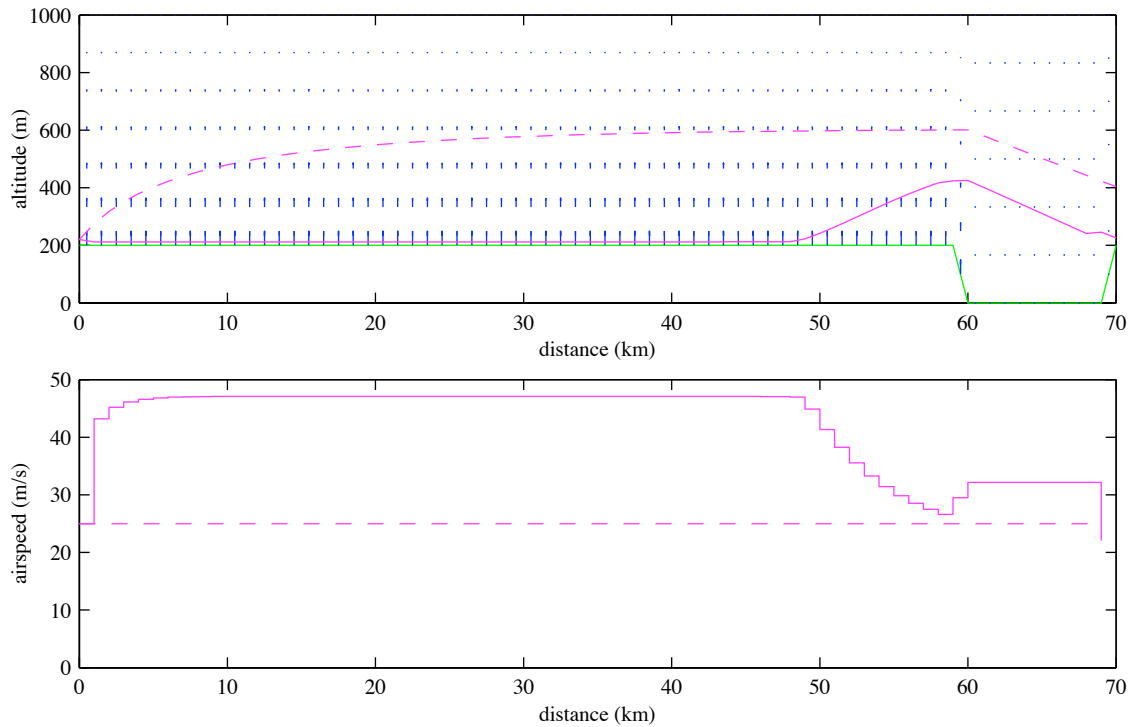
VII.   Conclusion

This paper has introduced a system to enable small uninhabited aerial vehicles to extract energy from the atmosphere. The $(LD)^2$ (long duration, long distance) flight which is enabled by autonomous energy extraction has the potential to greatly improve the ability of small and micro UAVs to fulfill current missions and may permit these vehicles to perform tasks which are currently impossible due to range and endurance limits.

A critical component of $(LD)^2$ flight is trajectory planning to exploit atmospheric lift. This paper has presented a methodology to generate these lift-exploiting trajectories. A point mass model for the aircraft is used and the flight is spatially discretized. A polynomial wind field is assumed and both vertical and horizontal wind components can be considered.

Optimal trajectories for a small autonomous glider (1m^2 wing area, 10kg mass) were generated for gliding
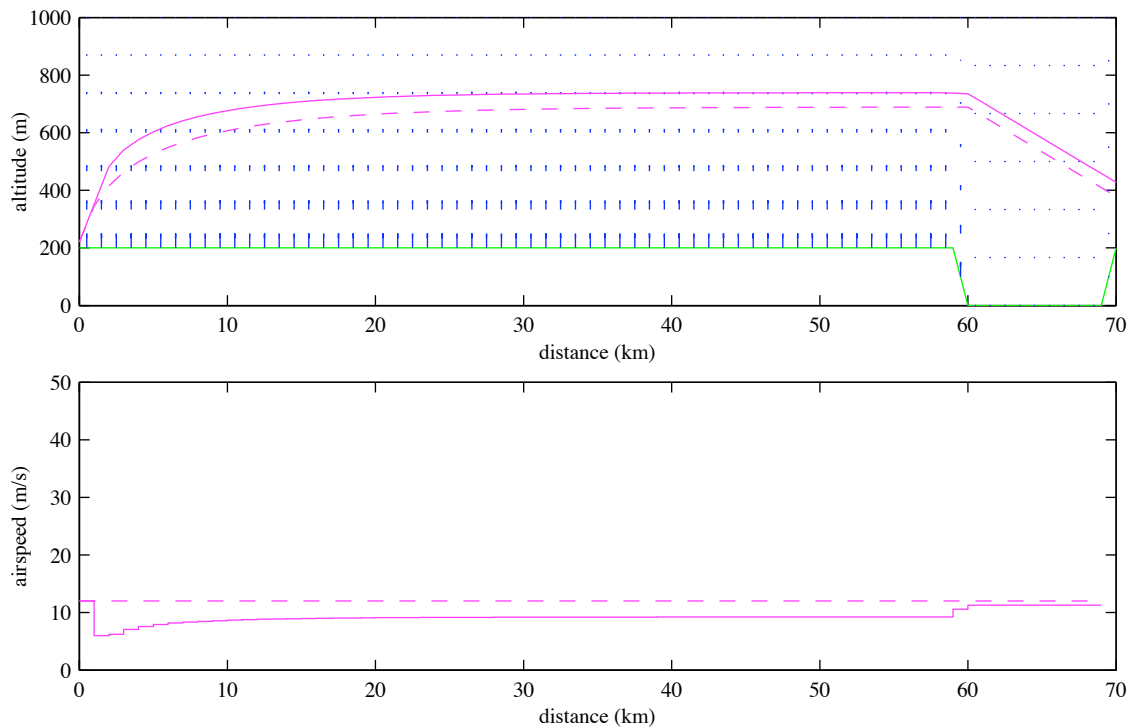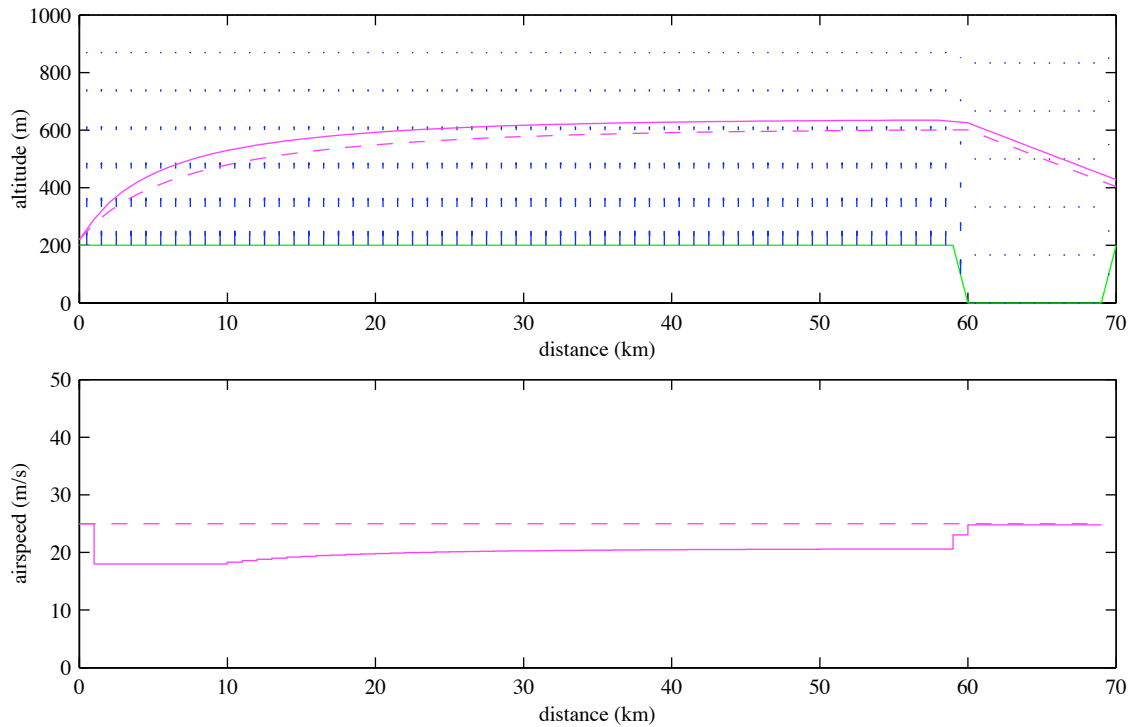
(a) small UAV

(b) high-performance sailplane

Figure 8. Optimal trajectory for minimum time to goal (solid magenta). Blue arrows show the wind field, terrain is shown as a green line. For comparison, the dashed magenta line shows the trajectory resulting from constant airspeed (at best L/D for each wing loading). The lower figure in each pair shows the optimal speed to fly in each segment, again with solid line showing speed to fly for the optimal trajectory and dashed line showing the speed for best L/D.

American Institute of Aeronautics and Astronautics Paper 2007-6737

(a) small UAV

(b) high-performance sailplane

Figure 9. Optimal trajectory for maximum energy at goal (solid magenta). Blue arrows show the wind field, terrain is shown as a green line. For comparison, the dashed magenta line shows the trajectory resulting from constant airspeed (at best L/D for each wing loading). The lower figure in each pair shows the optimal speed to fly in each segment, again with solid line showing speed to fly for the optimal trajectory and dashed line showing the speed for best L/D.

American Institute of Aeronautics and Astronautics Paper 2007-6737

flight along a 60km constant height ridge followed by a 10km gap crossing. The vertical component of wind speed varied approximately inversely with altitude above the ridge and was zero in the gap. Both minimum time and maximum final energy trajectories were considered, with the optimal minimum time trajectory showing significant improvement over the constant speed trajectory and the maximum energy trajectory also showing (somewhat smaller) improvement. For comparison, optimal trajectories were also computed for a modern high performance sailplane.

References

[1] Rayleigh, J. W. S., "The Soaring of Birds," *Nature*, Vol. 27, 1883, pp. 534–535.

[2] Rayleigh, J. W. S., "The Sailing Flight of the Albatross," *Nature*, Vol. 40, 1889, pp. 34.

[3] Boslough, M. B. E., "Autonomous Dynamic Soaring Platform for Distributed Mobile Sensor Arrays," Tech. Rep. SAND2002-1896, Sandia National Laboratories, Sandia National Laboratories, 2002.

[4] Kiceniuk, T., "Calculations on Soaring in Sink," *Technical Soaring*, Vol. 25, No. 4, October 2001, pp. 228–230.

[5] Patel, C. K. and Kroo, I., "Control Law Design for Improving UAV Performance using Wind Turbulence," *AIAA Aerospace Sciences Meeting and Exhibit*, AIAA Paper 2006-0231, American Institute of Aeronautics and Astronautics, Reno, Nevada, January 2006.

[6] "MM5 Community Model Homepage," .

[7] Hendricks, F., *Dynamic Soaring*, Ph.D. thesis, University of California, Los Angeles, Los Angeles, California USA, 1972.

[8] Sachs, G. and Mayrhofer, M., "Shear Wind Strength Required for Dynamic Soaring at Ridges," *Technical Soaring*, Vol. 25, No. 4, October 2001, pp. 209–215.

[9] Sachs, G., "Minimum Shear Wind Strength Required for Dynamic Soaring of Albatrosses," *Ibis*, Vol. 147, 2005, pp. 1–10.

[10] Zhao, Y. J., "Optimal Patterns of Glider Dynamic Soaring," *Optimal Control Applications and Methods*, Vol. 25, 2004, pp. 67–89.

[11] Wharington, J. M., "Heuristic Control of Dynamic Soaring," *5th Asian Control Conference*, 2004.

[12] Woolsey, C., Hagerman, G., and Morrow, M., "A Self Sustaining Boundary Layer Adapted System for Terrain Exploration and Environmental Sampling," Phase I final report, NASA Institute for Advanced Concepts, 2005.

[13] Kiceniuk, T., "Dynamic Soaring and Sailplane Energetics," *Technical Soaring*, Vol. 25, No. 4, October 2001, pp. 221–227.

[14] Kiceniuk, T., "A Variometer for Dynamic Soaring," *Technical Soaring*, Vol. 25, No. 4, October 2001, pp. 231–234.

[15] Pennycuick, C. J., "Gust Soaring as a Basis for the Flight of Petrels and Albatrosses (Procellariiformes)," *Avian Science*, Vol. 2, No. 1, 2002, pp. 1–12.

[16] Allen, M. J., "Autonomous Soaring for Improved Endurance of a Small Uninhabited Air Vehicle," *43rd AIAA Aerospace Sciences Meeting and Exhibit*, American Institute of Aeronautics and Astronautics, Reno, Nevada, January 2005.

[17] Allen, M. J. and Lin, V., "Guidance and Control of an Autonomous Soaring Vehicle with Flight Test Results," *AIAA Aerospace Sciences Meeting and Exhibit*, AIAA Paper 2007-867, American Institute of Aeronautics and Astronautics, Reno, Nevada, January 2007.

[18] MacCready Jr., P. B., "Optimum Airspeed Selector," *Soaring*, January-February 1958, pp. 10–11.

[19] Cochrane, J. H., "MacCready Theory with Uncertain Lift and Limited Altitude," *Technical Soaring*, Vol. 23, No. 3, July 1999, pp. 88–96.

[20] Reichmann, H., *Cross-Country Soaring*, Thomson Publications, Santa Monica, California, 1978.

[21] Arho, R., "Optimal Dolphin Soaring as a Variational Problem," *OSTIV Publication XIII*, Organisation Scientifique et Technique Internationale du Vol à Voile, 1974.

[22] Metzger, D. E. and Hedrick, J. K., "Optimal Flight Paths for Soaring Flight," *Journal of Aircraft*, Vol. 12, No. 11, 1975, pp. 867–871.

[23] Sandauer, J., "Some Problems of the Dolphin-Mode Flight Technique," *OSTIV Publication XV*, Organisation Scientifique et Technique Internationale du Vol à Voile, 1978.

[24] de Jong, J. L., "The Convex Combination Approach: A Geometric Approach to the Optimization of Sailplane Trajectories," *OSTIV Publication XVI*, Organisation Scientifique et Technique Internationale du Vol à Voile, 1981, pp. 182–201.

[25] Pierson, B. L. and Chen, I., "Minimum Altitude Loss Soaring in a Specified Vertical Wind Distribution," *NASA Conference Publication 2085, Science and Technology of Low Speed and Motorless Flight*, edited by P. W. Hanson, NASA, Hampton, Virginia, March 1979, pp. 305–318.

[26] Sander, G. and Litt, F. X., "On Global Optimal Sailplane Flight Strategy," *NASA Conference Publication 2085, Science and Technology of Low Speed and Motorless Flight*, edited by P. W. Hanson, NASA, Hampton, Virginia, March 1979, pp. 355–376.

[27] Anisi, D. A., Robinson, J. W. C., and Ogren, P., "On-line Trajectory Planning for Aerial Vehicles: a Safe Approach with Guaranteed Task Completion," *AIAA Guidance, Navigation and Control Conference*, AIAA Paper 2006-6107, American Institute of Aeronautics and Astronautics, Keystone, Colorado, August 2006.

[28] Schouwenaars, T., Feron, E., and How, J., "Safe Receding Horizon Path Planning for Autonomous Vehicles," *40th Allerton Conference on Communication, Control and Computing*, October 2002.

[29] Phillips, W. H., "Propulsive Effects due to Flight through Turbulence," *Journal of Aircraft*, Vol. 12, No. 7, July 1975, pp. 624–626.

[30] Lissaman, P. B. S. and Patel, C. K., "Neutral Energy Cycles for a Vehicle in Sinusoidal and Turbulent Vertical Gusts," *45th AIAA Aerospace Sciences Meeting and Exhibit*, AIAA Paper 2007-863, American Institute of Aeronautics and Astronautics, Reno, Nevada, January 2007.

[31]Klemp, J. B., "Research-Community Priorities for WRF-System Development," Tech. rep., WRF Research Applications Board, 2006.

[32]Haupt, S. E., Young, G., and Allen, C., "A Genetic Algorithm Method to Assimilate Sensor Data for a Toxic Contaminant Release," *Journal of Computers*, Vol. accepted for publication, 2007.

[33]DG Flugzeugbau GmbH, Bruchsal, Germany, *Flight Manual for the Sailplane DG-808S*, November 2003.

[34]Knauff, T., *Ridge Soaring the Bald Eagle Ridge*, Knauff and Grove Soaring Supplies, 3523 South Eagle Valley Road, Julian, PA 16844, 5th ed., 2003.